J Mater Sci (2017) 52:4197–4209

Effect of alloying on interfacial energy of precipitation/matrix in high-chromium martensitic steels

A. Fedoseeva[1,*], E. Tkachev[1], V. Dudko[1], N. Dudova[1], and R. Kaibyshev[1]

[1] *Belgorod State University, Pobeda 85, Belgorod, Russia 308015*

Received: 17 August 2016
Accepted: 30 November 2016
Published online: 7 December 2016

ABSTRACT

The effect of cobalt, tungsten, and boron on interfacial energy of precipitate/ferritic matrix in the 9% Cr martensitic steels on the base of creep tests at 650 °C under different applied stresses ranging from 80 to 220 MPa was investigated. An interfacial energy of $M_{23}C_6$ carbides, the Laves phase particles, and MX carbonitrides was estimated by comparison of theoretical curves obtained by Prisma software for the model steels for the exposure time of 2×10^4 h with experimental data measured by TEM in the gage sections of crept specimens. Addition of 3 wt% Co to Co-free 9Cr2W steel led to about 1.7 times increase in the interfacial energy of $M_{23}C_6$ carbides and MX carbonitrides, whereas Co did not effect on the interfacial energy of the Laves phase. Increasing W from 1.5 to 3 wt% in the Co-containing steels led to increase in the interfacial energy of the Laves phase up to 0.78 J m^{-2} under long-term exposure, whereas it did not effect on the interfacial energy of $M_{23}C_6$ carbides and MX carbonitrides. In the steel with increased B up to 0.012 wt% and decreased N to 0.007 wt%, a strong decrease in the interfacial energy of $M_{23}C_6$ carbides to 0.12 J m^{-2} occurred. Change in the interfacial energy of the precipitates was analyzed in comparison with coarsening rate constant.

Introduction

Heat-resistant steels with 9–12% Cr are widely used as structural materials for boilers, steam main tubes, and turbines of fossil power plants to increase thermal efficiency [1, 2]. The excellent creep resistance of these steels is attributed to the tempered martensitic lath structure (TMLS) consisting of prior austenite grains (PAG), packets, blocks, and laths and containing a high density of separate dislocations and a dispersion of secondary phase particles. $M_{23}C_6$-type carbides and MX carbonitrides (where M–Nb, V, and X–C, N) precipitate along boundaries and within the ferritic matrix, respectively, during tempering. $M_{23}C_6$ carbides exerting a high Zener drag force stabilize the TMLS [3–7], while MX carbonitrides are the obstacles for the movement of the dislocations [6, 7]. Degradation of the creep resistance after long-term service

Address correspondence to E-mail: fedoseeva@bsu.edu.ru

DOI 10.1007/s10853-016-0654-5

occurs due to the microstructure evolution. Nanoscale MX carbonitrides tend to transform into the coarse particles of Z phase within ferritic matrix; Ostwald ripening leads to the significant coarsening of $M_{23}C_6$ carbides; and the coarse Laves phase particles precipitated along high-angle boundaries during creep testing [6–9]. As a result, dynamic recovery occurs in the TMLS, and a well-defined subgrain structure replacing the dislocation structure of former martensite evolves finally [7].

Particle coarsening is observed to follow the well-known Ostwald ripening equation [10, 11]:

$$d^3 - d_0^3 = K_p(t - t_0), \quad (1)$$

where d_0 and d are the mean sizes of particles for time t_0 and t, respectively; K_p is the coarsening rate constant; the coefficient n depends on the coarsening mechanism; and $n = 3$ for the mechanism of the bulk diffusion assumed in the present model [10–12]. The interfacial energy γ between the matrix and the particles is very important characteristic of particle coarsening because it is included in the value of the coarsening rate constant K_p [12]:

$$K_p = \frac{8}{9}\frac{\gamma V_m^{\beta}}{\sum_{i=1}^{C}\frac{RT(x_i^{\beta}-x_i^{\alpha/\beta})^2}{x_i^{\alpha/\beta}D_i}}, \quad (2)$$

where V_m is the molar volume of the precipitate phase; D_i is the diffusion coefficient of element i in the matrix; x_i^{β} is the mole fraction of element i in the precipitate; and $x_i^{\alpha/\beta}$ is the mole fraction of element i at the precipitate/matrix interface. Bulk diffusion is assumed. Usually the value of γ is in the range 0.1–1 J m^{-2}, where the lowest values correspond to coherent particle/matrix interfaces and higher values correspond to incoherent interfaces [10–12]. The particles with coherent particle/matrix interfaces have higher coarsening resistance during creep that shift the recovery of the TMLS to longer times.

Thus, improved long-term creep strength could be achieved by slowing down the coarsening of $M_{23}C_6$ carbides, MX carbonitrides, and the Laves phase particles. An effective way to attain this goal is to slow down the diffusion by the additives, such as cobalt, tungsten, or/and boron. It was recently shown that Co additions significantly hinder the coarsening of $M_{23}C_6$ carbides and MX carbonitrides under creep conditions that result in superior creep resistance of the martensitic steels [13–16]. However, the mechanism of this positive effect from Co is not yet clear. Efficiency of W as alloying element in hindering the diffusion is much higher than that of Co. As a result, W and Mo are known as effective alloying additives to enhance creep resistance of the high-chromium martensitic steels. However, in contrast with cobalt, the tungsten and molybdenum have limited solubility within the ferrite, and their excessive content leads to the precipitation of such W/Mo-rich particles as Laves phase Fe_2(W, Mo) or M_6C carbides [1, 7, 9, 14–18]. Boron can replace carbon in $M_{23}C_6$ carbides that leads to two-phase separation $M_{23}C_6$ phase onto B-rich M_{23}(C,B)$_6$ and B-free particles. M_{23}(C, B)$_6$ particles are more resistant to the coarsening than B-free carbides that provides increased stability of the TMLS under creep conditions [1]. However, there is limited published data about the effect of these elements on the interfacial energy of precipitate/ferritic matrix [14–16]. The present work is aimed to establish the effect of alloying elements Co, W, and B on the interfacial energy of precipitate/matrix of $M_{23}C_6$ carbides, the Laves phase particles, and MX carbonitrides in the P92-type steels. The calculations of the particle growth kinetic using Prisma software and the comparison of experimental data with theoretically predicted coarsening behavior are used in order to determine the values of the interfacial energy.

Materials and methods

P92 steel and two 3% Co-modified P92-steels distinguished by W content (2 and 3 wt%) and denoted here as the Co-free 9Cr2W, the 9Cr3Co2W, and the 9Cr3Co3W steels were used. These steels contained conventional N of 0.05 wt% and were produced by air melting as 40 kg ingots. Also, the 3% Co-modified P92-type steel with lower N content of 0.007 wt% and increased B content of 0.012 wt%, which is denoted here as the 9Cr3Co1.5W0.012B steel, was used; it was prepared by vacuum induction melting. The chemical compositions of these steels are given in Table 1. Square bars were hot forged in the temperature interval range of 1150–1050 °C after homogenization annealing at 1100 °C for 1 h. All steels were normalized at 1050–1060 °C, air cooled, and subsequently tempered at 750 °C for 3 h. Details of the manufacturing process and heat treatment of these

Table 1 Chemical compositions of the steels studied (in wt%)

	C	Cr	Co	Mo	W	V	Nb	B	N	Si	Mn	Ni
Co-free 9Cr2W	0.10	8.75	–	0.51	1.6	0.2	0.07	0.005	0.05	0.17	0.54	0.21
9Cr3Co2W	0.12	9.3	3.1	0.44	2.0	0.2	0.06	0.005	0.05	0.08	0.2	0.04
9Cr3Co3W	0.12	9.5	3.2	0.45	3.1	0.2	0.06	0.005	0.05	0.06	0.2	0.04
9Cr3Co1.5W0.012B	0.10	9.0	2.8	0.57	1.5	0.2	0.05	0.012	0.007	0.12	0.4	0.24

steels were reported in the previous works [2, 9, 13, 14]. Flat specimens with a gage length of 25 mm and a cross section of 7 × 3 mm^2 and cylindrical specimens with a gage length of 100 and a 10 mm diameter were creep tested until rupture at a constant load at 650 °C and the initial applied stresses ranging from 220 to 80 MPa with a step of 20 MPa using ATS2330 lever arm machines.

The microstructural characterization was performed in the gage section of the crept specimens using a transmission electron microscope JEM-2100 (TEM) operated at 200 kV and equipped with an INCA energy-dispersive X-ray spectrometer (EDS) and a Quanta 600FEG scanning electron microscope. TEM foils were prepared by double jet electropolishing using a solution of 10% perchloric acid in glacial acetic acid. Extraction replicas were used for precipitate analysis. The specimens were mechanically polished by emery paper and 3 μm silica suspension, and then etched using a solution of 3 ml hydrochloric acid and 1 g picric acid in 10 ml of ethanol. The size distribution and the mean radius of the secondary phase particles were estimated by counting from 150 to 250 particles per specimen on at least 15 arbitrarily selected typical TEM images for each data point. The transverse lath size was measured on at least six arbitrarily selected typical TEM images for each data point by a linear intercept method, counting all clearly defined boundaries. The dislocation density was estimated by counting individual dislocations revealed by TEM within lath interiors per unit area. Identification of the precipitates in TEM investigations was performed based on a combination of EDS composition measurements of the metallic elements and indexing of electron diffraction patterns using TEM.

The particle coarsening kinetic was calculated using Prisma software on the base Calphad Database Calculation with the kinetic MOBFE1 and the thermodynamic TCFE6 databases. The model compositions consisting of Fe, C, Cr, Mo, W, and Co in accordance with the chemical composition of the steels studied (Table 1) were used for estimating the coarsening of $M_{23}C_6$ carbides and the Laves phase particles assuming that a grain boundary is a nucleation site. In order to estimate the coarsening of MX carbonitrides, the model compositions consisting of Fe, C, N, Cr, V, Nb, W, and Co were used; a nucleation site was assumed to be on a dislocation. The interfacial energy was estimated by the comparison of calculated kinetic of the particle growth using the Prisma software and the experimental data.

Experimental results

Microstructures in tempered condition

The typical microstructures of the 9% Cr steels after normalizing and tempering are presented in Fig. 1, and the structural parameters are summarized in Table 2. It is worth noting that there are some differences in the microstructures and the dispersions of second phases in the steels studied. The complex structure consisting of the TMLS and the subgrains is observed in the Co-free 9Cr2W and 9Cr3Co2W steels [19], whereas increasing W content as well as increasing B content provides the formation of the full TMLS in the 9Cr3Co3W and 9Cr3Co1.5W0.012B steels [19, 20]. An average size of the PAGs is practically the same in all steels, whereas it is insignificantly larger in the steel with low N content that can be associated with higher normalizing temperature (1050 vs. 1060 °C). A lath thickness is nearly the same in the steels.

Nanoscale $M_{23}C_6$ carbides decorate the boundaries of PAGs, blocks, packets, and laths in all steels studied after tempering at 750 °C. In the 9Cr3Co1.5W0.012B steel, the average size of $M_{23}C_6$ carbides is smaller than in other steels that can be attributed to the formation of B-rich carbides with higher coarsening resistance. Thermo-Calc software predicts two-phase separation of $M_{23}C_6$ carbides to B-rich $M_{23}(C, B)_6$ and B-free $M_{23}C_6$ carbides in the steel with high B content [21]. Fine MX carbonitrides

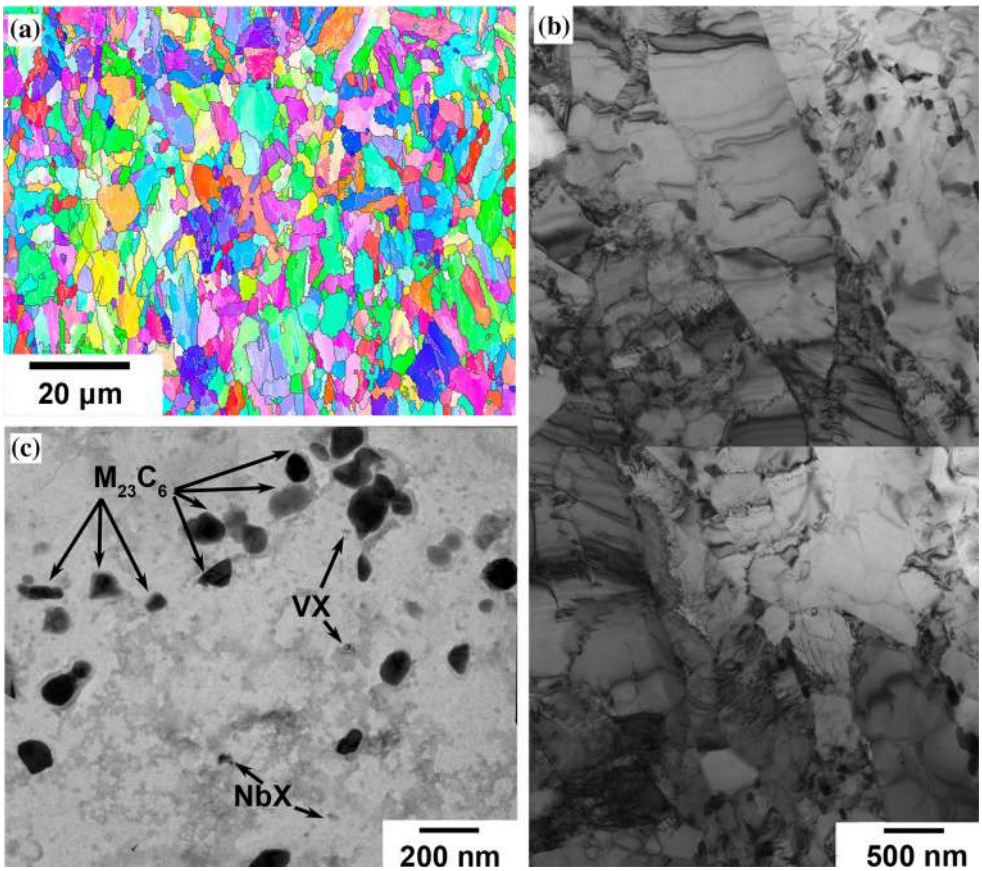

Figure 1 The typical structure of the 9% Cr martensitic steel after normalizing at (1050 ± 10) °C and tempering (750 ± 10) °C using EBSD technique (**a**) and TEM of foils (**b**) and replicas (**c**).

Table 2 Structural parameters of the steels studied after normalizing and tempering

Steel	D_{PAG} (μm)	d_{lath} (μm)	$\rho_{\perp} \times 10^{14}$ (m^{-2})	$d_{particle}$ (nm)		
				$M_{23}C_6$	NbX	VX
Co-free 9Cr2W	20 ± 2	0.45 ± 0.15	2.5 ± 1	85 ± 25	35 ± 10	26 ± 5
9Cr3Co2W	10 ± 1	0.38 ± 0.15	2.0 ± 1	90 ± 30	40 ± 10	20 ± 5
9Cr3Co3W	15 ± 2	0.38 ± 0.15	2.6 ± 1	90 ± 30	40 ± 10	20 ± 5
9Cr3Co1.5W0.012B	26 ± 5	0.30 ± 0.10	2.6 ± 1	70 ± 25	47 ± 10	49 ± 16

precipitate within the ferritic matrix. The average size of the Nb-rich and V-rich MX particles is nearly the same in all steels studied (Table 2), whereas the volume fraction of the MX particles in the 9Cr3Co1.5W0.012B steel is tenfold decreased in comparison with other steels due to negligibly small amount of the V-rich MX phase resulted from low N content in this steel (Table 3).

In the steel with 3 wt% W content, the precipitation of W-rich fine Laves phase (~90 nm) and coarse M_6C phase (~300 nm) particles along PAG boundaries takes place under tempering condition. However, the volume fractions of these particles are negligible.

Creep behavior

Figure 2 shows the creep rupture time versus applied stress curves for all steels studied at 650 °C under the applied stresses ranging from 220 to 80 MPa. Any alloying of the base P92 steel results in improving the creep resistance: thus, time to rupture increases from $<10^2$ h to $2 \div 3.5 \times 10^3$ h at 140 MPa, and from 2×10^3 h to $\geq 10^4$ h at 100 MPa (Fig. 2). Increasing W content from 2 to 3% as well as decreasing N content from 0.05 to 0.007% with increasing B content up to 0.012 wt% result in increasing the creep strength only at the short-term creep tests, whereas the creep

Table 3 The volume fraction of second phases at 750 and 650 °C calculated using the Thermo-Calc software for the steels studied

	At 750 °C			At 650 °C		
	$M_{23}C_6$	Laves	MX	$M_{23}C_6$	Laves	MX
Co-free 9Cr2W	0.01855	–	0.00344	0.01933	0.00685	0.00342
9Cr3Co2W	0.02299	–	0.00336	0.02349	0.01230	0.00337
9Cr3Co3W	0.02316	0.0124	0.00338	0.02362	0.02432	0.00339
9Cr3Co1.5W0.012B	0.01779	–	0.00037	0.01865	0.00879	0.00038

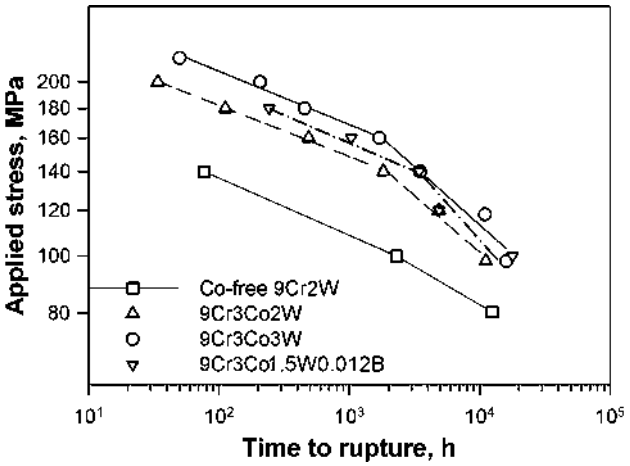

Figure 2 Creep properties of the 9% Cr martensitic steels.

strength at the long-term creep tests is nearly the same for the 9% Cr Co-containing steels. All steels studied demonstrate well-defined creep strength breakdown. In the steel with N content of 0.05 wt%, creep strength breakdown appears after 2000 h of the creep tests, whereas decreasing N content to 0.007% with increasing B content to 0.012% shifts the appearance of creep strength breakdown from 2000 to 3500 h. Recently, the depletion of W from the solid solution due limited solubility of W and Mo atoms in the ferrite matrix was established to be one of the reason for breakdown appearance [22]. In 2000 h of creep, W content in the steels with 0.05 wt% N reaches the equilibrium value that leads to the coarsening of $M_{23}C_6$ carbides and the Laves phase particles [22]. The formation of B-rich carbides $M_{23}(C,B)_6$ with higher coarsening resistance is able to overlap the depletion of W from the solid solution and to slow down the structure degradation during creep [16, 21, 22].

Crept microstructures

The appearance of creep strength breakdown led to distinctly different structural changes during the short-term creep and the long-term creep. The TMLS of all steels examined remained during the short-term creep (Fig. 3a), whereas during the long-term creep the transformation of the TMLS into the subgrain structure occurred (Fig. 3b).

It is known [1, 2, 4, 9, 13, 16, 22] that $M_{23}C_6$ carbides and the Laves phase particles located along high-angle (PAG, packet, blocks) and low-angle (lath) boundaries play the important role in the retarding the transformation of the TMLS into the subgrain structure by exerting Zener forces on these boundaries that stabilize the TMLS under creep conditions.

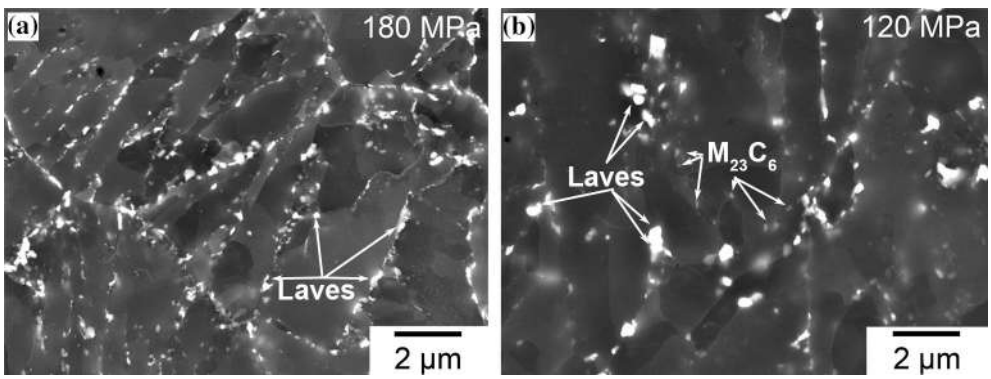

Figure 3 The typical microstructures of the 9% Cr martensitic steels after short-term creep (**a**) and long-term creep (**b**) tests (the 9Cr3Co2W steel is shown after creep tests at 650 °C under the applied stresses of 180 and 120 MPa).

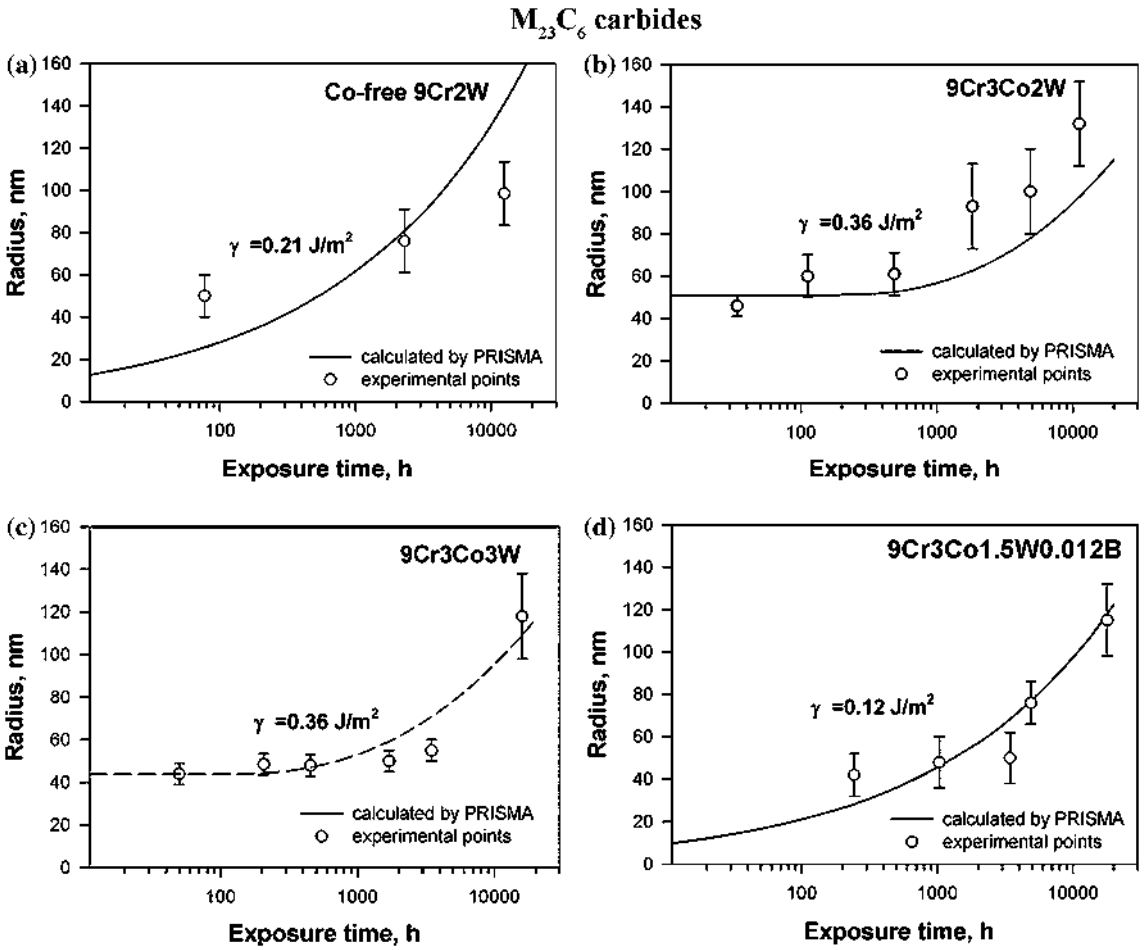

Figure 4 The time dependence of the particle size of $M_{23}C_6$ carbides during creep: **a** the 9Cr2W steel; **b** the 9Cr3Co2 W steel; **c** the 9Cr3Co3 W steel; and **d** the 9Cr3Co3W0.012B steel. *Circle points* are the experimental data for the steels studied; *solid lines* are calculated curves obtained by Prisma software for the model steels.

The Laves phase particles precipitate during the short-term creep along the PAG and lath boundaries in all steels. However, the character of coarsening of $M_{23}C_6$ carbides and the Laves phase particles is significantly different for the steels examined. Figures 4, 5, and 6 show the coarsening of $M_{23}C_6$ carbides, the Laves phase particles, and MX carbonitrides, respectively, under creep conditions.

$M_{23}C_6$ carbides

Coarsening of $M_{23}C_6$ carbides in the 9Cr3Co2 W steel occurred faster than in other steels studied during creep testing (Fig. 4). A mean radius of these carbides increased to 100–125 nm after 500 h in the 9Cr3Co2W steel, whereas in other steels with 3% Co, the mean radius remained less than 50 nm up to rupture time of ~4000 h. In the Co-free 9Cr2W steel, the mean radius of $M_{23}C_6$ carbides increased from 60 to 100 nm at the transition from the short-term creep to the long-term creep. Therefore, increasing W content up to 3% as well as decreasing N content to 0.007% with increasing B content to 0.012% enhances the coarsening resistance of $M_{23}C_6$ carbides under short-term creep conditions. At the same time, under long-term creep conditions, the average dimensions of $M_{23}C_6$ carbides in all steels studied became essentially the same.

Laves phase particles

Increasing W content from 1.5 to 3 wt% led to the change in the precipitation behavior of the Laves phase particles (Fig. 5). In the 9Cr3Co1.5W0.012B steel, the Laves phase particles initially precipitated having large radius more than 80 nm and coarsened

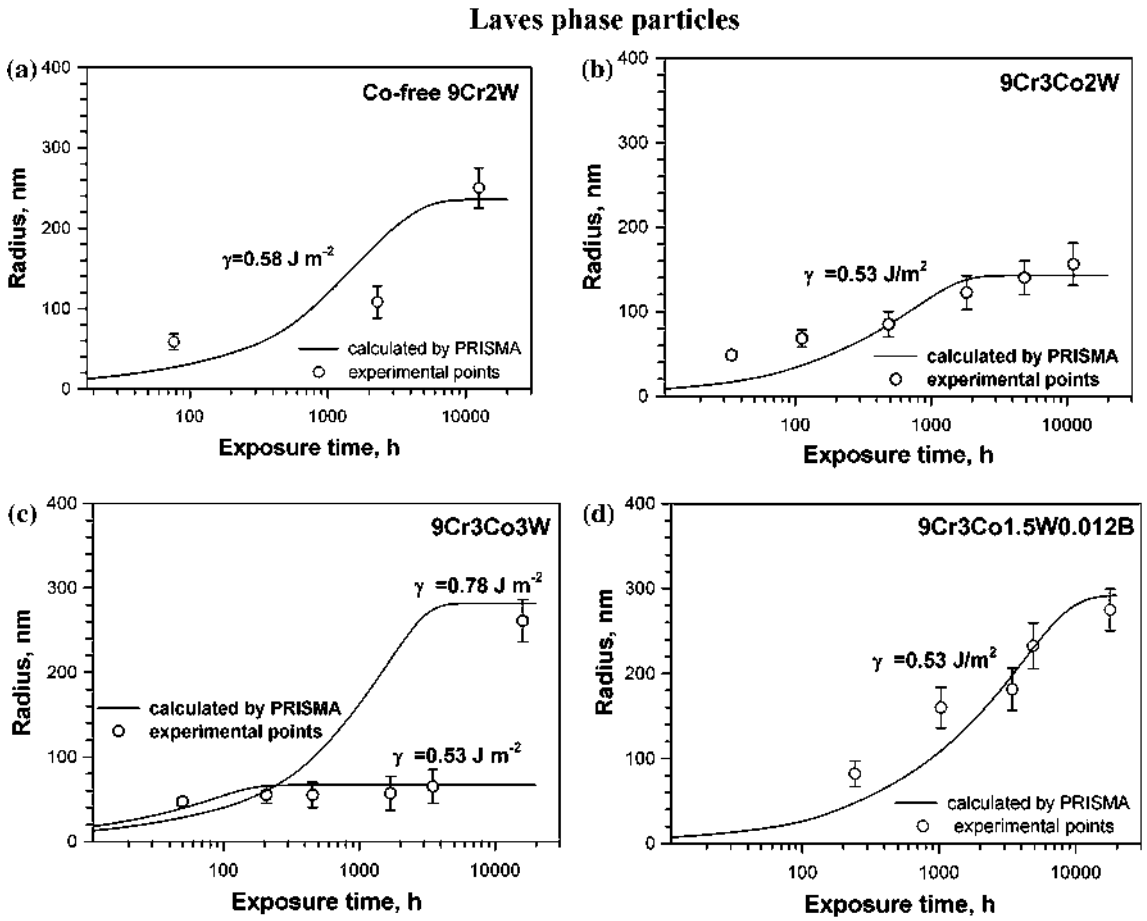

Figure 5 The time dependence of the particle size of Laves phase during creep: **a** the 9Cr2W steel; **b** the 9Cr3Co2W steel; **c** the 9Cr3Co3W steel; and **d** the 9Cr3Co3W0.012B steel. *Circle points* are the experimental data for the steels studied; *solid lines* are calculated curves obtained by Prisma software for the model steels.

to approximately 230-nm radius during 18,000 h of exposure, whereas in the 9Cr3Co2W and 9Cr3Co3W steels, the initial radius of these particles was less and was 40–50 nm. In the 9Cr3Co3W steel, the Laves phase particles retained their size of ~50 nm up to 4000 h. Then, the rapid coarsening of the Laves phase particles started to occur, and their average radius attained ~225 nm after creep rupture during ~16,000 h. In contrast, in the 9Cr3Co2W steel with 2% W, the Laves phase particles coarsened with a high rate under short-term creep conditions and reached 150–250 nm radius after creep rupture at ~11,000 h. The difference in the coarsening behavior was associated with the volume fractions of these particles. Thus, in the 9Cr3Co1.5W0.012B steel, the volume fraction of Laves phase was the smallest (0.89% as calculated by the Thermo-Calc software, Table 3) that provides the low number of the particle nuclei and their rapid growth. Increasing W content led to the increase in the volume fraction of Laves phase up to 2.39% for the 9Cr3Co3W steel (Table 3).

MX carbonitrides

These particles were very stable under creep conditions in all steels studied and remained their size ranging 30-nm radius (Fig. 6). Well-known transformation of fine V-rich MX carbonitrides into a coarse *Z* phase was observed only in the Co-containing steels (not shown in Fig. 6). In the Co-containing steels, the several small isolated particles enriched by Cr (~43 wt%), V (~26 wt%) and Nb (~20 wt%) with an average size of 50–70 nm were revealed after creep test at 120 MPa for 4869 h for the 9Cr3Co2W steel and 100 MPa for 15,998 and 17,859 h for the 9Cr3Co2W and 9Cr3Co1.5W0.012B steels, respectively [23]. These particles having a round shape were identified as *Z* phase (CrVN) [24, 25]. In the

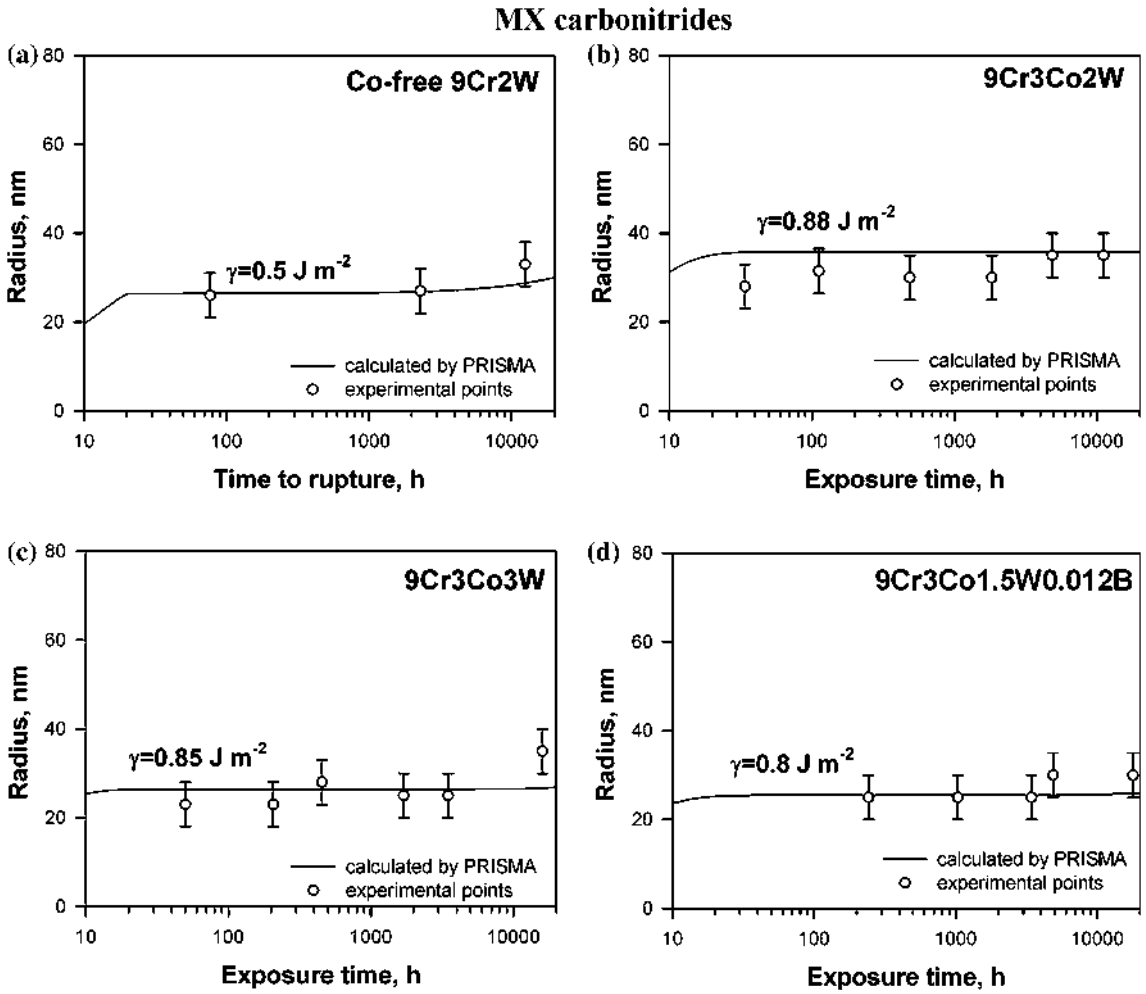

Figure 6 The time dependence of the particle size of MX carbonitrides during creep: **a** the 9Cr2W steel; **b** the 9Cr3Co2W steel; **c** the 9Cr3Co3W steel; and **d** the 9Cr3Co3W0.012B steel. *Circle points* are the experimental data for the steels studied; *solid lines* are calculated curves obtained by Prisma software for the model steels.

9Cr3Co2W steel, this transformation followed by growth of *Z* phase particles finished at rupture time $>10^4$ h and resulted in the full replacement of the nanoscale V-rich MX carbonitrides by the coarse particles of *Z* phase [23].

Comparison between model and experiment

The calculation of the particle growth kinetic using the Prisma software was carried out (Figs. 4, 5, 6) for the model steels consisting of Fe, C, Cr, Mo, W, Co/Fe, C, N, Cr, V, Nb, W, and Co in accordance with the chemical composition of the steels studied for the exposure time of 2×10^4 h. On the base of comparison of these theoretically predicted curves with experimental data (particle sizes measured using TEM in the gage sections of the crept specimens after creep tests at 650 °C under the different applied stresses), the values of the interfacial energy γ of $M_{23}C_6$ carbides, the Laves phase particles, and MX carbonitrides were estimated (Figs. 4, 5, 6).

$M_{23}C_6$ carbides

As can be observed from Fig. 4a, the calculated curve and the experimental data for the Co-free 9Cr2W steel are in a good agreement that evidences for the correctness of the given value of 0.21 J m^{-2} of the interphase energy (Fig. 4). The +3% Co additives increase the interfacial energy from 0.21 to 0.36 J m^{-2} (Fig. 4a–c). For the 9Cr3Co1.5W0.012B steel, significantly decreased interfacial energy of 0.12 J m^{-2} is obtained (Fig. 4d). The interfacial energy ranging of 0.2–0.5 J m^{-2} indicates the incoherent boundary

between $M_{23}C_6$ carbides and the ferritic matrix. $M_{23}C_6$ carbides were observed in the microstructure as precipitates on the PAG and lath/subgrain boundaries. However, in the steel with high B content, the interfacial energy of 0.12 J m^{-2} indicates coherent boundary between $M_{23}C_6$ carbides and the ferritic matrix while these particles are found to precipitate on similar locations in the microstructure as carbides in other steels examined.

Laves phase particles

Good agreement with the experimental data for the steels with W content of 1.5–2% is obtained with the interfacial energy of 0.53–0.58 J m^{-2} (Fig. 5a, b, d). Increasing W content from 1.5 to 3 wt% increases the value of the interfacial energy from 0.53 to 0.78 J m^{-2} after 5000 h of exposure at 650 °C (Fig. 5c). The interfacial energy of 0.5–0.8 J m^{-2} indicates the incoherent boundary between the Laves phase particle and the ferritic matrix that is in accordance with the microstructure observations.

MX carbonitrides

The Co-free 9Cr2W steel demonstrates the lowest interfacial energy of 0.5 J m^{-2} (Fig. 6a), whereas varying of Co, W, B, and N contents leads to the increase in the interfacial energy to 0.8–0.88 J m^{-2} (Fig. 6b–d). The value of 0.5 J m^{-2} for the Co-free 9Cr2W steel is in accordance with other investigations [10–12] and indicates incoherent boundary between MX carbonitrides and the ferritic matrix. The +3 wt% Co additives increase the value of the interfacial energy from 0.5 to 0.88 J m^{-2}. Increasing W content and decreasing N content with increasing B content do not affect the interfacial energy, and it is in range of 0.8–0.85 J m^{-2}.

Discussion

The interfacial energy γ between the precipitates and the ferritic matrix affects particle coarsening and their final size under creep conditions. However, despite the different values of the estimated interfacial energy of $M_{23}C_6$/matrix and MX/matrix for different steels, the sizes of $M_{23}C_6$ carbides and MX carbonitrides under long-term creep conditions are nearly the same in all steels studied. This is attributed to the influence of other parameters, such as the diffusion coefficients of different elements in the matrix, on the particle coarsening in accordance with Eq. (2) assuming that the mole fractions of elements in the precipitate and the precipitate/matrix interface are constant under long-term creep.

The coarsening rate constant, K_p, is evaluated using Eq. (1) for the precipitates in the steels studied (Fig. 7). The values of K_p for $M_{23}C_6$ carbides, Laves phase particles, and MX carbonitrides are presented in Figs. 7 and 8.

$M_{23}C_6$ carbides

As can be observed from Figs. 7a and 8a, alloying of the Co-free 9Cr2W steel by 3 wt% Co leads to twofold increase in the coarsening rate constant K_p that is in accordance with increase in the interfacial energy. Increasing W from 2 to 3 wt% leads to twofold increase in the coarsening rate constant while the interfacial energy of $M_{23}C_6$ carbides is the same for the steels with 2 and 3 wt% W (Figs. 7a, 8a). In the 9Cr3Co1.5W0.012B steel with decreased N content and increased B content, three times decrease in the interfacial energy of $M_{23}C_6$/matrix, in comparison with the 9Cr3Co2W steel, is in agreement with two times decreased the coarsening rate constant (Fig. 8a).

Nevertheless, taking into account that the mean sizes of $M_{23}C_6$ carbides are nearly the same after the creep tests for about 2×10^4 h in all steels studied, the values of K_p for all steels can be considered as nearly the same. So, though the +3% Co addition to the Co-free 9Cr2W steel results in +70% increase in the interfacial energy, its insignificant influence on the coarsening rate constant can be attributed to the significant effect of Co on slowing down the diffusion-controlled processes that is in agreement with other investigations [9], wherein the interfacial energy increases.

The low value of the interfacial energy of $M_{23}C_6$ carbides is related to high content of boron in the 9Cr3Co1.5W0.012B steel. Boron is not included in the calculations for the coarsening model in the Prisma software. It is well known [26] that B atoms segregate in the vicinity of PAG boundaries and stabilize the fine distribution of $M_{23}C_6$ carbides during creep [26] that reduces the rate of Ostwald ripening of these particles. The boron segregations have strong effect on the grain boundary diffusion [26]. However, the

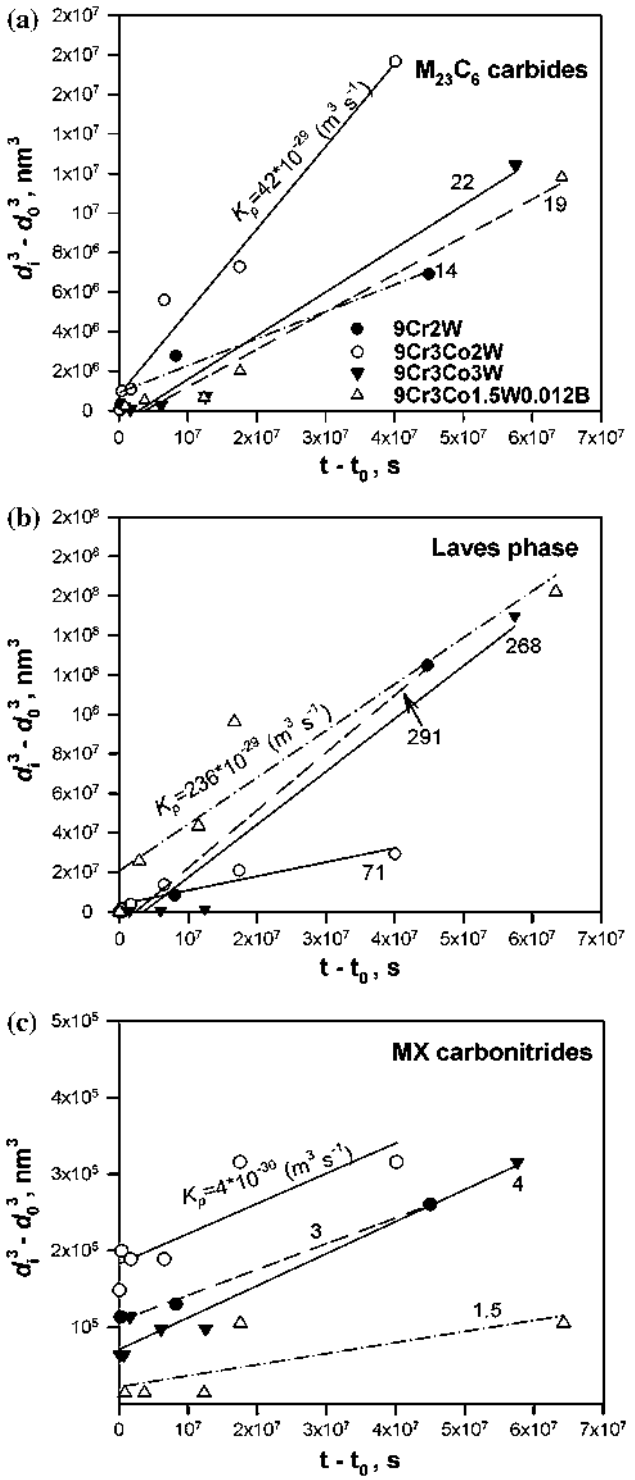

Figure 7 The time dependence of the precipitate size at 650 °C in the gage sections for **a** $M_{23}C_6$ carbides, **b** the Laves phase particles, and **c** MX carbonitrides. *Numbers* mean the coarsening rate constant for different steels.

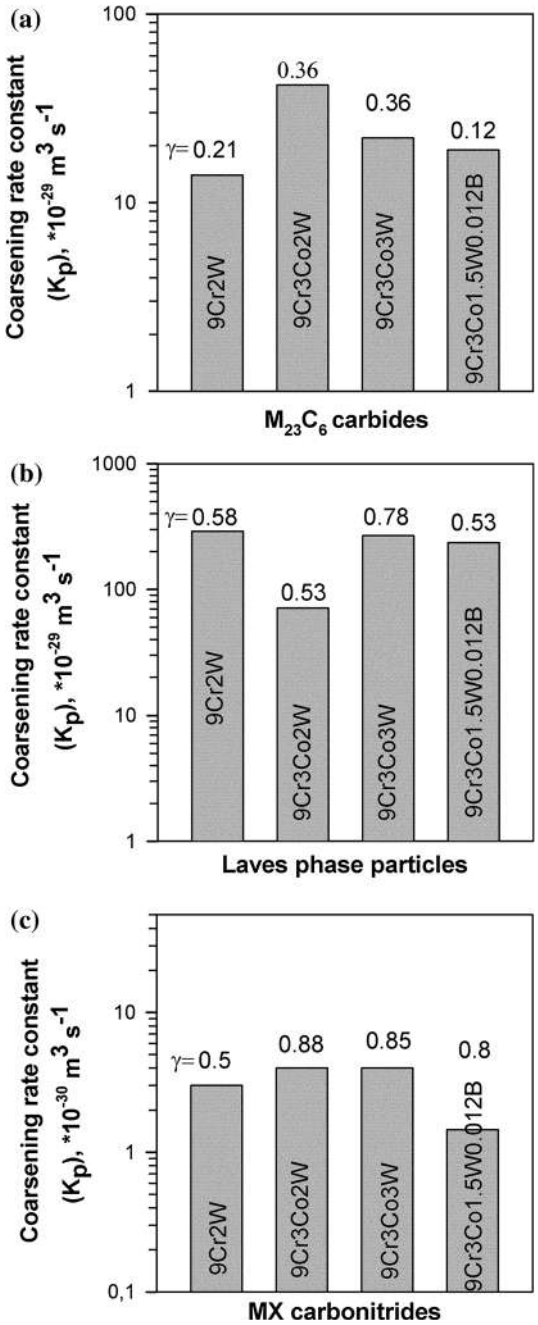

Figure 8 Coarsening rate constant of $M_{23}C_6$ carbides (**a**), Laves phase particles (**b**), and MX carbonitrides (**c**) in the steels studied after creep tests at 650 °C. *Numbers* indicate the values of the interfacial energy γ (J m^{-2}) from Figs. 4, 5, and 6.

coarsening rate constant is similar with other steels examined and is $\sim 2 \times 10^{-28}$ m^3 s^{-1}. As revealed earlier [21], small coarsening resistance of these

carbides in this steel can be attributed to high Σ(Ni + Mn) content, which increases the diffusivities used in Eq. (2).

Laves phase

The +3 wt% Co additive significantly reduces the coarsening rate constant (by four times), whereas the interfacial energy γ of the Laves phase particles does not change obviously (Figs. 7b, 8b). So, the +3% Co additives enhance the coarsening resistance of Laves phase in spite of its slight effect on the interfacial energy. On the other hand, further increasing W from 2 to 3% in Co-containing steels leads to the fourfold acceleration of Ostwald ripening of the Laves phase particles (Figs. 7b, 8b), which correspond to +50% increase in the interfacial energy γ from 0.53 to 0.78 J m^{-2}. It is necessary to notice the discrete character of the interfacial energy γ of the Laves phase particles in the 9Cr3Co3W steel, which increases from 0.53 to 0.78 J m^{-2} at the transition from the short-term creep to the long-term creep conditions, where the rapid coarsening of the Laves phase particles occurs.

Decreasing N and increasing B contents do not affect the interfacial energy of the Laves phase particles in comparison with the 9Cr3Co2W steel (0.53 J m^{-2}), whereas the coarsening rate constant significantly increases up to the level of the Co-containing steel with 3% W (Fig. 8b) that can be attributed to the low volume fraction of these particles and their quick growth.

MX carbonitrides

As can be observed from Fig. 8c, no accelerated coarsening of MX carbonitrides occurred in the Co-modified 9Cr3Co2W steel while ~1.8 times increasing the interfacial energy was revealed. This effect of Co can be resulted from the facilitating of the transformation of V-rich MX carbonitrides into the Z phase. As well known, Z phase is not a problem for Co-free P92-type steels because the formation of this phase can occur after long-term exposure of 3–4 × 10^4 h [24, 25], whereas in the Co-containing steels [23], this transformation takes place after short-term exposure of 5–10 × 10^3 h. Cobalt addition leads to destabilizing of MX carbonitrides by increasing their interfacial energy. On the other hand, the mean size of MX carbonitrides is nearly the same for the Co-free and 9Cr3Co2W steels that indicates that Co reduces the diffusion coefficients of V and Nb in the ferritic matrix.

In the 9Cr3Co1.5W0.012B steel with the low N content, the low volume fraction of V-rich MX carbonitrides (0.04%) is seemed to be the main reason for decreasing the coarsening rate constant of the MX particles in comparison with other steels, which contain ~0.34% MX phase (Fig. 8c).

So, particle coarsening is determined not only by the value of the interfacial energy γ but also by the diffusion coefficients of different elements in the matrix. Alloying of the 9Cr steels has a strong influence on the interfacial energy γ as well as on the diffusion coefficients.

Conclusions

The effect of cobalt, tungsten, and boron on the interfacial energy of precipitate/ferritic matrix in the 9% Cr martensitic steels on the base of creep tests at 650 °C was investigated. The main results can be summarized as follows:

(1) Alloying of the Co-free steel by 3 wt% Co results in improving creep resistance: thus, time to rupture increases from $<10^2$ h to 2 ÷ 3.5 × 10^3 h at 140 MPa and from 2 × 10^3 to $\geq 10^4$ h at 100 MPa.

(2) Addition of 3 wt% Co to the Co-free 9Cr2W steel leads to about 1.7 times increase in the interfacial energy γ of $M_{23}C_6$ carbides and MX carbonitrides that correspond to fourfold and 1.5-fold increase in the coarsening rate constant of these phases, respectively, whereas Co does not effect on the interfacial energy of Laves phase.

(3) Increasing W from 2 to 3 wt% in the Co-containing 9Cr3Co2W and 9Cr3Co3W steels leads to increase in the interfacial energy γ of Laves phase up to 0.78 J m^{-2} under long-term exposure. W addition does not effect on the interfacial energy of $M_{23}C_6$ carbides and MX carbonitrides. The combination of 3% Co and 2% W is able to provide minimal coarsening rate of the Laves phase particles during creep.

(4) Increased B up to 0.012 wt% strong decreases the interfacial energy of $M_{23}C_6$ carbides to 0.12 J m^{-2}, whereas no effect on the interfacial

energy of Laves phase and MX phases is revealed.

Acknowledgements

The authors acknowledge with gratitude the financial support received through the Russian Science Foundation, under Grant No. 14-29-00173. The authors are grateful to the staff of the Joint Research Center, Belgorod State University, for their assistance with instrumental analysis.

Compliance with ethical standards

Conflict of interest statement The authors declare that they have no conflict of interest.

References

[1] Abe F, Kern TU, Viswanathan R (2008) Creep resistant steels: Part I. Woodhead Publishing in Materials, Cambridge, England, pp 403–420

[2] Kaybyshev RO, Skorobogatykh VN, Shchenkova IA (2010) New martensitic steels for fossil power plant: creep resistance. Phys Met Metall 109:186–200

[3] Kitahara H, Ueji R, Tsuji N, Minamino Y (2006) Crystallographic features of lath martensite in low-carbon steel. Acta Mater 54:1279–1288

[4] Ghassemi Armaki H, Chen R, Maruyama K, Igarashi M (2010) Premature creep failure in strength enhanced high Cr ferritic steels caused by static recovery of tempered martensite lath structures. Mater Sci Eng A 527:6581–6588

[5] Abe F (2009) Analysis of creep rates of tempered martensitic 9%Cr steel based on microstructure evolution. Mater Sci Eng A 510–511:64–69

[6] Kostka A, Tak K-G, Hellmig RJ, Estrin Y, Eggeler G (2007) On the contribution of carbides and micrograin boundaries to the creep strength of tempered martensite ferritic steels. Acta Mater 55:539–550

[7] Abe F (2005) Effect of fine precipitation and subsequent coarsening of Fe_2W Laves phase on the creep deformation behavior of tempered martensitic 9Cr–W steels. Metall Mater Trans A 36:321–331

[8] Taneike M, Sawada K, Abe F (2004) Effect of carbon concentration on precipitation behavior of $M_{23}C_6$ carbides and MX carbonitrides in martensitic 9Cr steel during heat treatment. Metall Mater Trans A 35:1255–1261

[9] Dudova N, Plotnikova A, Molodov D, Belyakov A, Kaibyshev R (2012) Structural changes of tempered martensitic 9% Cr–2% W–3% Co steel during creep at 650 °C. Mat Sci Eng A 534:632–639

[10] Prat O, Garcia J, Rojas D, Sauthoff G, Inden G (2013) The role of Laves phase on microstructure evolution and creep strength of novel 9% Cr heat resistant steels. Intermetallics 32:362–372

[11] Prat O, Garcia J, Rojas D, Carrasco C, Inden G (2010) Investigations on the growth kinetics of Laves phase precipitates in 12% Cr creep-resistant steels: experimental and DICTRA calculations. Acta Mater 58:6142–6153

[12] Hald J, Korcakova L (2003) Precipitate stability in creep resistant ferritic steels—experimental investigations and modelling. ISIJ Int 43(3):420–427

[13] Kipelova A, Belyakov A, Kaibyshev R (2012) Laves phase evolution in a modified P911 heat resistant steel during creep at 923 K. Mater Sci Eng A 532:71–77

[14] Fedorova I, Belyakov A, Kozlov P, Skorobogatykh V, Shenkova I, Kaibyshev R (2014) Laves-phase precipitates in a low-carbon 9% Cr martensitic steel during aging and creep at 923 K. Mater Sci Eng A 615:153–163

[15] Isik MI, Kostka A, Yardley VA, Pradeep KG, Duarte MJ, Choi PP, Raabe D, Eggeler G (2015) The nucleation of Mo-rich Laves phase particles adjacent to $M_{23}C_6$ micrograin boundary carbides in 12% Cr tempered martensite ferritic steels. Acta Mater 90:94–104

[16] Ghassemi Armaki H, Chen R, Maruyama K, Igarashi M (2011) Creep behavior and degradation of subgrain structures pinned by nanoscale precipitates in strength-enhanced 5–12 Pct Cr ferritic steels. Metall Mater Trans A 42:3084–3094

[17] Tsuchida Y, Okamoto K, Tokunaga Y (1995) Improvement of creep rupture strength of high Cr ferritic steel by addition of W. ISIJ Int 35:317–323

[18] Li Q (2006) Precipitation of Fe_2W Laves phase and modeling of its direct influence on the strength of a 12Cr–2W steel. Metall Mater Trans A 37:89–97

[19] Fedoseeva A, Dudova N, Glatzel U, Kaibyshev R (2016) Effect of W on tempering behaviour of a 3%Co modified P92 steel. J Mat Sci 51:9424–9439. doi:10.1007/s10853-016-0188-x

[20] Fedorova I, Kostka A, Tkachev E, Belyakov A, Kaibyshev R (2016) Tempering behavior of a low nitrogen boron-added 9%Cr steel. Mater Sci Eng A 662:443–455

[21] Kaibyshev R, Mishnev R, Tkachev E, Dudova N (2016) Effect of Ni and Mn of the creep behavior of 9–10% Cr steels with low N and high B. Trans Indian Inst Met 69(2):203–210

[22] Fedoseeva A, Dudova N, Kaibyshev R (2016) Creep strength breakdown and microstructure evolution in a 3%Co modified P92 steel. Mater Sci Eng A 654:1–12

[23] Fedoseeva A, Dudova N, Kaibyshev R (2016) Effect of tungsten on a dispersion of M(C, N) carbonitrides in 9% Cr steels under creep conditions. Trans Indian Inst Met 69(2):211–215

[24] Cipolla L, Danielsen HK, Venditti D, Di Nunzio PE, Hald J, Somers MA (2010) Conversion of MX nitrides to Z-phase in a martensitic 12% Cr steel. Acta Mater 58:669–679

[25] Danielsen HK, Di Nunzio PE, Hald J (2013) Kinetics of Z-phase precipitation in 9–12 pct Cr steels. Metall Mater Trans A 44:2445–2452

[26] Abe F (2008) Precipitate design for creep strengthening of 9% Cr tempered martensitic steel for ultra-supercritical power plants. Sci Technol Adv Mater 9(1):3002. doi:10.1088/1468-6996/9/1/013002